



COMPARISON OF CFD AND EMPIRICAL MODELS FOR PREDICTING WALL TEMPERATURE AT SUPERCRITICAL CONDITIONS OF WATER

S. Anand^a, S. Suresh^a, R. Dhanuskodi^b, D. Santhosh Kumar^{b,*}

^a Department of Mechanical Engineering, National Institute of Technology, Trichy, Tamilnadu, 620015, India

^b Research & Development Department, Bharath Heavy Electricals, Ltd., Trichy, Tamilnadu. 620014, India

ABSTRACT

The present work investigates the wall temperature prediction at supercritical pressure of water by CFD and compares the prediction of CFD and that of 11 empirical correlations available in literature. Supercritical-water heat transfer experimental data, covering a mass flux range of 400-1500 kg/m²s, heat flux range of 150-1000 kW/m², at pressure 241 bar and diameter 10 mm tube, were obtained from literature. CFD simulations have been carried out for those operating conditions and compared with experimental data. Around 362 experimental wall temperature data of both heat transfer enhancement and heat transfer deterioration region have been taken for comparison. A visual Basic program has also been developed to predict wall temperature for the selected empirical correlations and compared with those of 362 experimental data. Ranking based on the deviation with experimental data is also listed.

Keywords: SST-k ω model, heat transfer enhancement, heat transfer deterioration, supercritical water

1. INTRODUCTION

The Advanced Ultra Supercritical Boilers will be the next generation of boilers because it possesses various advantages like relatively low energy cost, low pollutant emission and high efficiency. The Advanced Ultra Supercritical Boilers are aimed to operate at a pressure and temperature of 300 bar and 700°C respectively with a higher thermal efficiency up to 46%. As the water walls operate at conditions above the critical point of water, which is 221 bar and 374°C, the fluid will remain as a single phase. Thus no departure from nucleate boiling or dry-out can occur. However in the vicinity of this critical point, strong variations of water properties combined with a high heat flux or low mass flux can lead to heat transfer deterioration (HTD), which consequently causes a severe increase of wall temperature (Cheng *et al.*, 2003). Thus, the study of heat transfer behavior at pseudocritical region is extremely important. It has been found that the fluid temperature and pressure in the evaporator region varies between 342°C & 440°C and 270 & 290 bar respectively at Boiler Maximum Continuous Rating condition. The pseudocritical temperature at 270 and 290 bar is found to be 392°C (2177.39 kJ/kg) and 399°C (2204.21 kJ/kg). This indicates that somewhere in the evaporator region the fluid crosses the pseudocritical temperature. Therefore, it is indeed necessary to study the heat transfer behavior at pseudocritical temperature at the desired pressure range and determine the inner wall temperature.

Various experimental investigations have been performed at supercritical conditions with water flowing upward in circular pipes under intense electrical heating (Bishop *et al.*, 1964; Yamagata *et al.*, 1972; Jackson and Hall, 1979; Zhu *et al.*, 2009) and published empirical correlations applicable for predicting the heat transfer at supercritical conditions of water. Each correlation is applicable for the specified range of operating parameters. These correlations are used for determining the inner wall temperature. Several established dimensionless correlations for heat transfer of supercritical water namely, Dittus-Boelter, 1930; McAdams, 1942, Bishop *et al.*, 1964; Shitsman, 1968; Ornaty *et al.*, 1971; Yamagata *et al.*, 1972; Jackson

and Hall, 1979; Watts and Chou, 1982; Griem, 1996; Zhu *et al.*, 2009; Mokry *et al.*, 2011 etc., are available in the literature to predict the wall temperature. Nevertheless, the comparisons of experimental data and correlations still show considerable disagreement at the regimes of the heat transfer deterioration. This is because the derivation of all the existing correlations was based on their own experimental dataset. This is one of the main drawbacks of empirical correlations. Numerical studies indeed become necessary in order to obtain more insight into the heat transfer behavior in supercritical fluids.

The accuracy of numerical simulations of heat transfer in supercritical may depend on the choice of turbulence models. A number of investigations about the application of turbulence models in the numerical simulation of flow and heat transfer for supercritical water have been carried out. But, standard wall functions of the turbulence models are not capable to predict heat transfer deterioration. Jaromin and Anglart (2013) found that SST k- ω model is capable to predict heat transfer deterioration close to the experimental results. Wen and Gu (2011) also validated few turbulent models and found that SST k- ω is more accurate than other models. Zhi *et al.* (2016) used SST k- ω model for predicting convective heat transfer to hydro carbon fuel at supercritical pressure and assured that it performs well compared to all other turbulence models under supercritical pressure. He also employed the SST k- ω model in his analysis and validated with experimental results and showed that SST k- ω model is capable for predicting the heat transfer enhancement and heat transfer deterioration. In the present work, simulations were carried out using various turbulence models available in Ansys-Fluent to gain confidence.

The purpose of the present work is to numerically simulate the experimental conditions consisting of 362 data points available in literature for a range of parameters such as heat flux, mass flux, bulk fluid enthalpy, pressure, and tube diameter and compare the wall temperature predicted by CFD and 11 empirical correlations with the experimental data.

* Corresponding author. Email: santhoshkumar@bhel.in

1.1 Definitions of terms and properties of Supercritical water

Critical point is the point where the distinction between the liquid and gas (or vapor) phases disappears, i.e., both phases have the same temperature, pressure and volume (Fig. 1, Piro and Duffey, 2005). The critical point is characterized by the phase state parameters T_{cr} , P_{cr} and V_{cr} , which have unique values for each pure substance.

Pseudocritical point (characterized with P_{pc} and T_{pc}) is a point at a pressure above the critical pressure and at a temperature ($T_{pc} > T_{cr}$) corresponding to the maximum value of the specific heat for this particular pressure.

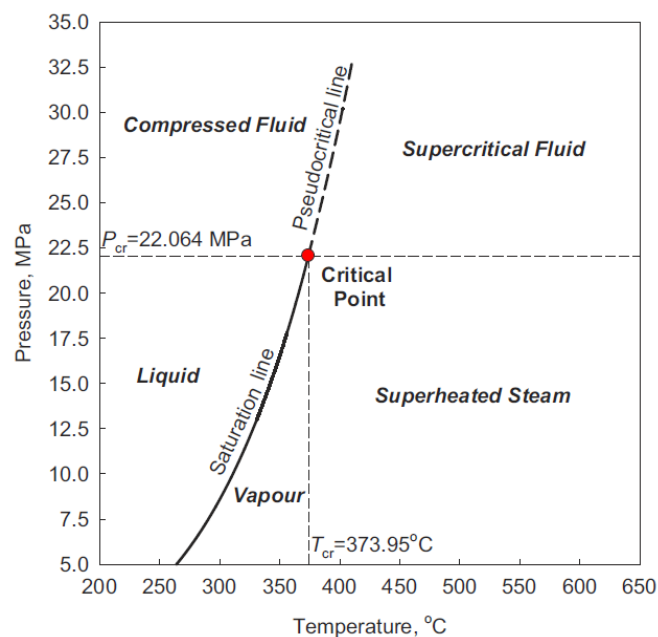


Fig. 1 Pressure-Temperature diagram of water in the critical region (Piro & Duffey, 2005).

Supercritical fluid is a fluid at pressures and temperatures that are higher than the critical pressure and critical temperature.

Supercritical steam (“steam”) is actually supercritical water because at supercritical pressures there is no difference between phases. However, this term is widely used in literature in relation to supercritical steam generators and turbines.

Normal heat transfer (NHT) is characterized by the Heat Transfer Coefficient (HTC) is similar to those of convective heat transfer at subcritical condition that occurs far away from pseudocritical regime and are closely matches with the HTC calculated using Dittus-Boelter equation “Eq. (1)”

$$Nu = 0.0243 Re^{0.8} Pr^{0.4} \quad (1)$$

Heat transfer enhancement (HTE) is characterized by higher values of the wall heat transfer coefficient compared to those at the normal heat transfer regime and hence lower values of wall temperature within some part of a test section or within the entire test section.

Heat transfer deterioration (HTD) is characterized by lower values of the wall heat transfer coefficient compared to those at the normal heat transfer regime and hence has higher values of wall temperature within some part of a test section or within the entire test section. Fig. 2 (Piro and Duffey, 2005) shows the variation of thermo-physical properties for water at 250 bar. The large variation in properties like density, specific heat, viscosity and thermal conductivity occur within +/- 25°C from the pseudo-critical temperature (384.9°C). This large variation influence heat transfer leading to initial heat transfer enhancement or deterioration depending on local conditions.

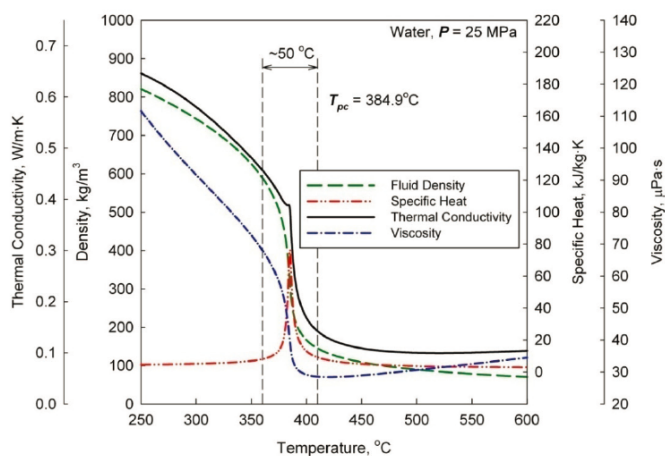


Fig. 2 Properties variation of water within pseudo-critical region at 250 bar (Piro and Duffey, 2005).

2. NUMERICAL METHODS

2.1 Geometry

In the present work, vertical smooth tube of ID 10 mm and length 4 m has been chosen for validation for which experimental results are available in the literature Mokry *et al.*, 2010 and Mokry *et al.*, 2011. Therefore, the computational test parameters considered in the present work are same as experiments conducted in Mokry *et al.*, 2010 and Mokry *et al.*, 2011. All the simulations in the present work are carried out using ANSYS Fluent 17.2. A 2D axis symmetry geometry has been modeled and shown in Fig. 3.

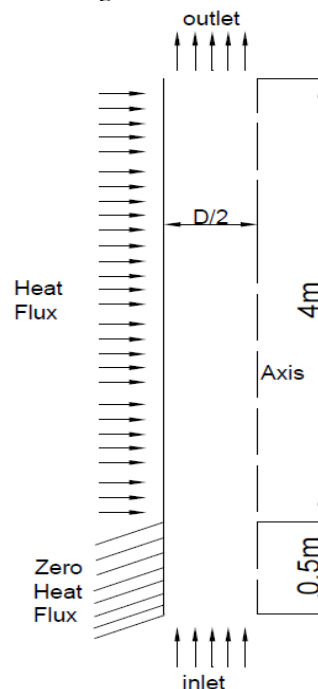


Fig. 3 Computational geometry

Since the wall temperature is uniform around the circumference of the vertical tube, a 2D model with axis-symmetry has been chosen for simulation in order to reduce the computational time. To take care of entrance effects, a 0.5m of additional length is also provided without heat flux to make the flow fully developed. The physical boundary conditions of the geometry are as follows: a uniform mass flux with inlet fluid temperature is specified at the inlet and a uniform heat flux is applied around the wall boundary for the heated length and zero heat flux is applied on the unheated length of wall boundary. The pressure outlet setting in the Fluent is used as outlet boundary condition and the symmetry condition is used for the axis.

2.2 Governing Equations

The basic governing equations, including the conservations of mass (continuity equation), momentum and energy, together with SST k- ω method is used to simulate the unique and complicated turbulent heat transfer characteristics at supercritical pressure (Marcin *et al.*, 2017 and Zhi and Chen, 2011).

$$\frac{\partial(\rho u_i)}{\partial x_i} = 0 \quad (2)$$

$$\frac{\partial(\rho u_i u_j)}{\partial x_j} = \rho g_i - \frac{\partial p}{\partial x_i} + \frac{\partial \tau_{ij}}{\partial x_j} + \frac{\partial}{\partial x_j} (-\overline{\rho u_i' u_j'}) \quad (3)$$

where,

$$\tau_{ij} = \mu \left(\frac{\partial u_i}{\partial x_j} + \frac{\partial u_j}{\partial x_i} - \frac{2}{3} \delta_{ij} \frac{\partial u_k}{\partial x_k} \right)$$

$$\frac{\partial \rho h}{\partial t} + \frac{\partial \rho h u_i}{\partial x_i} = \frac{\partial p}{\partial t} + u_i \frac{\partial p}{\partial x_i} + \left[\mu \left(\frac{\partial u_i}{\partial x_j} + \frac{\partial u_j}{\partial x_i} \right) - \frac{2}{3} \mu \frac{\partial u_k}{\partial x_k} \delta_{ij} \right] \frac{\partial u_i}{\partial x_j} + \frac{\partial}{\partial x_i} \left(\alpha \frac{\partial T}{\partial x_i} \right) + S_h \quad (4)$$

$$S_h = -\overline{(\rho u_i' u_j')} \frac{\partial u_i}{\partial u_j} - \frac{\partial \overline{\rho u_i' h}}{\partial x_j}$$

$$\frac{\partial \overline{\rho u_i' h}}{\partial x_j} = -\left(\frac{\mu_t}{\sigma_h} \right) \left(\frac{\partial h}{\partial x_i} \right) \text{ and}$$

the Reynolds stress term $\overline{\rho u_i' h}$ can be presented by turbulence models. By using Boussinesq approximation, the turbulent shear stress can be found from the following equation in which Reynolds stresses are related to the average velocity gradient

$$-\overline{\rho u_i' u_j'} = \mu_t \left(\frac{\partial u_i}{\partial x_j} + \frac{\partial u_j}{\partial x_i} - \frac{2}{3} \delta_{ij} \frac{\partial u_k}{\partial x_k} \right) - \frac{2}{3} \delta_{ij} \rho k$$

where,

μ_t is turbulent viscosity which is flow property; not a fluid property. In the present work, SST k- ω model is used,

$$\text{here, } \mu_t = \rho \frac{k}{\omega}$$

k- ω equations are derived from transport equations empirically for turbulent kinetic energy(k) and specific turbulent dissipation rate (ω).

$$\frac{\partial}{\partial t} (\rho k) + \frac{\partial}{\partial x_i} (\rho k u_i) = \frac{\partial}{\partial x_j} \left[\Gamma_k \frac{\partial k}{\partial x_j} \right] + G_k - Y_k + S_k \quad (5)$$

and

$$\frac{\partial}{\partial t} (\rho \omega) + \frac{\partial}{\partial x_i} (\rho \omega u_i) = \frac{\partial}{\partial x_j} \left[\Gamma_\omega \frac{\partial \omega}{\partial x_j} \right] + G_\omega - Y_\omega + S_\omega \quad (6)$$

G_k -generation of turbulence kinetic energy due to mean velocity gradients, G_ω - generation of turbulence kinetic energy at ω , Y_M and Y_ω - dissipation of k and ω , Γ_k and Γ_ω - effective diffusivity of k and ω , S_k, S_ω - user defined source terms. The governing differential equations are solved using the finite volume method. The QUICK scheme is used for approximating the convection terms in momentum and energy equations. The SIMPLE procedure is chosen to couple pressure and velocity. The algebraic equations are solved with ADI methodology. As already mentioned, fluid properties also abruptly change with pressure and temperature, therefore NIST Refprop which is an inbuilt program in Fluent has been used to compute fluid properties. The simulations are stopped when the convergence criteria become less than 10^{-6} so as to assure the enough accuracy level. In the present work, a number of turbulence models like SST k- ω , Low re - ϵ , RNG k- ϵ , Standard k- ϵ and Realizable models have been examined. Two numerical case studies were conducted for choosing the best turbulent models, Case I low $q/G=0.27$ & Case II high $q/G=0.67$. In case I, heat flux 141 kW/m², mass flux 504 kg/m²s and pressure 241 bar and Case II heat flux 334 kW/m², mass flux 499 kg/m²s and pressure 241 bar were used (Mokry *et al.*, 2011). In both studies, Mokry's *et al.*, 2011 experimental wall temperatures was compared with wall temperature predicted by various turbulence models. Fig. 4 In case I, all the models were closely matches with experiment data. Fig. 5 In case II, where q/G is high, causes heat transfer deterioration, only SST k- ω model follows the wall temperature trend with experiment data. All other models not able to predict sharp rise in wall temperature. Therefore, in the present work SST k- ω model has been used for all the computations.

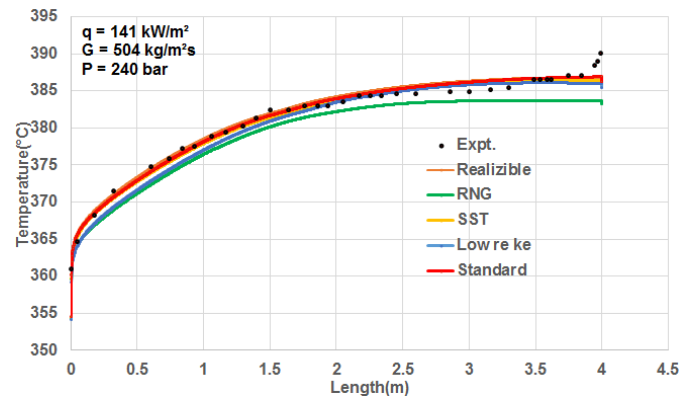


Fig. 4 Case I- comparison of various turbulent models at low $q/G=0.27$ (Mokry *et al.*, 2011).

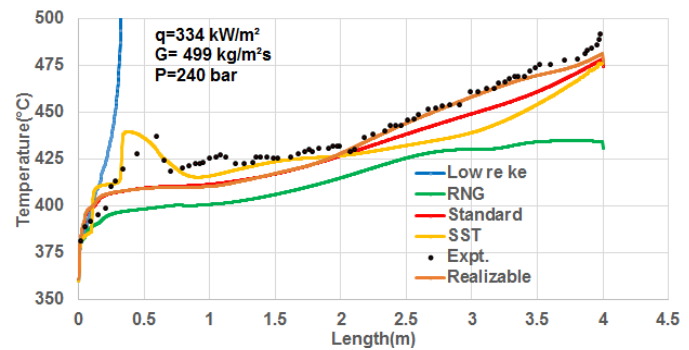


Fig. 5 Case II- comparison of various turbulent models at high $q/G=0.67$ (Mokry *et al.*, 2011).

2.3 Grid independence study and validation

As the accuracy of results depends upon the fineness of the grid, great care is required for selecting the grid size. More fineness of the grid increases the computational time. Therefore, grid independence study has been carried out to select the appropriate size of the grid. Any further refinement of the mesh doesn't change the solution. The test has been conducted for the geometry shown in Fig. 3 with various grid size of 60×1200, 80×1200, 100×1200, 120×1200, 140×1200 (radial nodes × axial nodes). Since the change in the parameters in radial direction is larger than the axial direction, non-uniform nodes with a successive ratio of 1.02 in the radial direction to have dense mesh near the wall and uniform nodes in the axial direction were used. Fig. 6 shows the zoomed view of computational mesh to represent fine mesh near the wall and coarse mesh near the axis. The additional 0.5 m length (shown in Fig. 3) is separately divided in to 120×300 grid nodes. In order to choose the appropriate mesh, simulation has been carried out for the experimental operating condition of with pressure 241 bar, heat flux 141 kW/m², mass flux of 504 kg/m² with various mesh sizes (Mokry *et al.*, 2011). The obtained wall temperature for various meshes are plotted and compared with experimental data as shown in Fig. 7. It is found that the temperature for meshes 120×1200 and 140×1200 closely matches with experimental data. Also, any further refinement of mesh does not alter the solution. Therefore 120×1200 mesh has been chosen for all the computations. In order to gain confidence, two validations have also been carried out for the pressure 241 bar, heat flux 190 kW/m² and mass flux 498 kg/m²s & pressure 241 bar, heat flux 334 kW/m² and mass flux 499 kg/m²s. Wall temperature is plotted against the length of the tube and compared with experimental wall temperature of represented in Fig. 8.(Mokry *et al.*,2010) & Fig. 9 (Mokry *et al.*,2011). These shows that the present simulation model is appropriate.

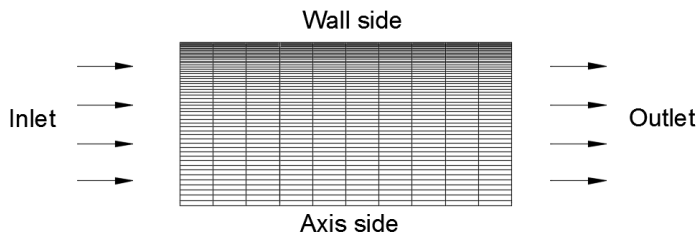


Fig. 6 Zoomed view of computational mesh

3. RESULTS AND DISCUSSION

3.1 Experiment based empirical correlations in literature

For predicting the heat transfer in turbulent convective heat transfer and for heat transfer at supercritical conditions, following experiment based empirical correlations are available in literature. Dittus - Boelter (1930) introduced a heat-transfer correlation at subcritical pressure for forced convection which is still universally used and is given by

$$Nu_b = 0.023 Re_b^{0.8} Pr_b^{0.4} \quad (5)$$

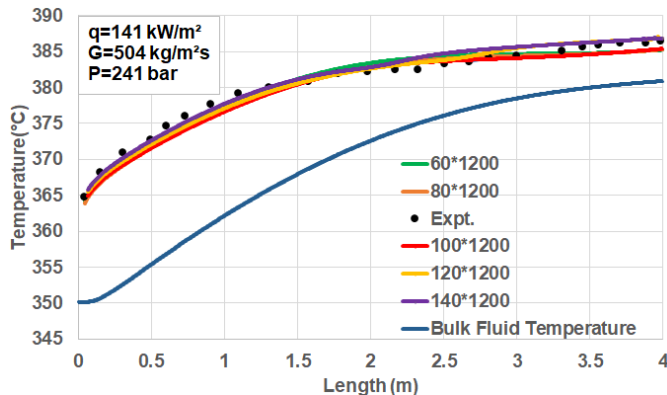


Fig. 7 Grid independence study for the case of pressure 241 bar, mass flux 504 kg/m² s, heat flux 141 kW/m² (Mokry *et al.*, 2011).

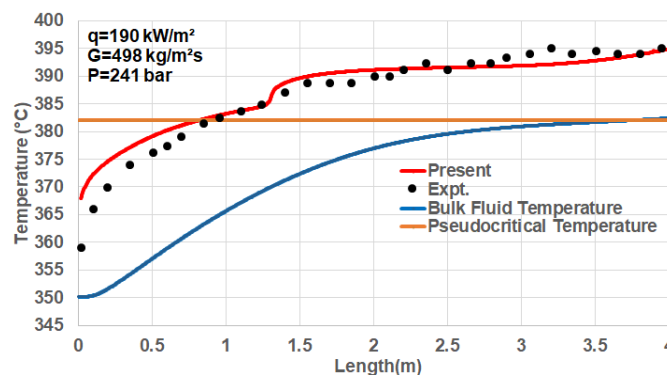


Fig. 8 Validation of present numerical simulation with experimental result of Mokry *et al.* (2010) for $q/G = 0.38$.

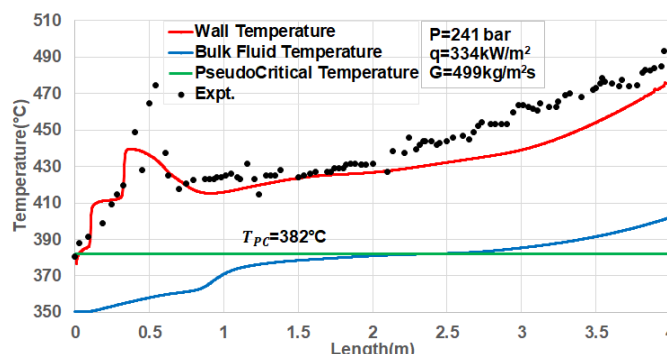


Fig. 9 Validation of present numerical simulation with experimental result of Mokry *et al.* (2011) for $q/G = 0.67$.

McAdams (1942) proposed to use the Dittus - Boelter (1930) equation in the following form for forced convective heat transfer in turbulent flows

$$Nu_b = 0.0243 Re_b^{0.8} Pr_b^{0.4} \quad (6)$$

Bishop *et al.* (1964) conducted experiments in supercritical water flowing upward inside bare tubes in the following range of operating parameters: $P=228 - 276$ bar, $T_b = 282 - 527^\circ\text{C}$, $G = 651 - 3662$ kg/m² s, and $q = 0.31$ to 3.46 MW/m² and proposed the following equation

$$Nu_x = 0.0069 Re_x^{0.9} \overline{Pr}_x^{0.66} \left(\frac{\rho_w}{\rho_b}\right)_x^{0.43} \left(1 + 2.4 \frac{D}{x}\right) \quad (7)$$

Shitsman, (1968) analyzed the heat transfer experimental data of supercritical water flowing inside tubes and then generalized these data with the Dittus-Boelter type correlation:

$$Nu_b = 0.023 Re_b^{0.8} Pr_{min}^{0.8} \quad (8)$$

The subscript "min" means minimum Pr value, i.e., either the Pr value evaluated at the bulk fluid temperature or the Pr value evaluated at the wall temperature.

Ornatsky *et al.* (1971) performed an experiment and recommended the following correlation:

$$Nu = 0.023 Re^{0.8} Pr_{min}^{0.8} \left(\frac{\rho_w}{\rho_b}\right)^{0.3} \quad (9)$$

Yamagata *et al.* (1972) performed an experiment and recommended the following correlation:

$$Nu_b = 0.0135 Re_b^{0.85} Pr_b^{0.8} F_c, \quad (10)$$

where $F_c = 1.0$ for $E > 1$, $F_c = 0.67 Pr_{pc}^{0.05} (\overline{c_p}/c_{pb})^{n_1}$ for $0 < E < 1$.

$$F_c = (\overline{c_p}/c_{pb})^{n_2} \text{ for } E < 0$$

$$n_1 = -0.77(1 + 1/Pr_m) - 0.53 \text{ and } n_2 = 1.44(1 + 1/Pr_m) - 0.53$$

Jackson and Hall (1979) performed experimental investigations of heat transfer to supercritical carbon dioxide in both upward and downward directions in a vertical circular tube and arrived at a correlation given below

$$Nu = 0.0183 Re_b^{0.82} \overline{Pr}^{0.5} \left(\frac{\rho_w}{\rho_b}\right)^{0.3} \left(\frac{\overline{c_p}}{c_{pb}}\right)^n \quad (11)$$

Where, $n = 0.4$ for $T_b < T_w$ and for $1.2T_{pc} < T_b < T_w$

$$n = 0.4 + 0.2 \left(\frac{T_w}{T_{pc}} - 1\right) \text{ for } T_b < T_{pc} < T_w$$

$$n = 0.4 + 0.2 \left(\frac{T_w}{T_{pc}} - 1\right) \left[1 - 5 \left(\frac{T_b}{T_{pc}} - 1\right)\right] \text{ for } T_{pc} < T_b < 1.2T_{pc} \text{ and } T_b < T_w$$

Watts and Chou (1982) developed an empirical correlation for vertical upward and downward flow. For the vertical upward flow, the correlation takes the form :

$$Nu_b = \begin{cases} Nu_{var} (7000\varphi)^{0.295}, & \text{if } 10^{-4} \leq \varphi \\ Nu_{var} (1 - 3000\varphi)^{0.295}, & \text{if } 10^{-5} \leq \varphi \leq 10^{-4} \end{cases} \quad (12)$$

$$Nu_{var} = 0.021 Re_b^{0.8} \overline{Pr}^{0.55} \left(\frac{\rho_w}{\rho_b}\right)^{0.35}$$

and the buoyancy parameter is defined as $\varphi = \overline{Gr}_b / (Re_b^{2.7} \overline{Pr}_b^{0.5})$

Griem (1996) presented correlation for forced convection heat transfer at critical and supercritical pressures in tubes in the following form:

$$Nu_b = 0.0169 Re_b^{0.8356} Pr_b^{0.432} \quad (13)$$

Zhu *et al.* (2009) investigated the heat transfer characteristics of steam-water two-phase flow in vertical upward tube in the range of pressure from 90 to 300 bar, mass velocity from 600 to 1200 kg/(m² s), and heat flux at inner wall from 200 to 600kW/m² and provided a Nusselt number correlation as

$$Nu_b = 0.0068 Re_b^{0.90} \overline{Pr}_b^{0.63} \left(\frac{\rho_w}{\rho_b}\right)^{0.17} \left(\frac{k_w}{k_b}\right)^{0.29} \quad (14)$$

Mokry *et al.* (2011) developed an empirical correlation in supercritical water flowing upward in a 10mm diameter tube at 240 bar, inlet temperature from 320 to 350 °C, mass flux ranged from 200 to 1500

kg/m² s and heat fluxes up to 1250 kW/m². The final form of correlation is given below

$$Nu_b = 0.0061 Re_b^{0.904} \overline{Pr}_b^{-0.684} \left(\frac{\rho_w}{\rho_b}\right)^{0.564} \quad (15)$$

3.2. Comparison of metal temperature predictions by CFD and empirical correlations

In an effort to make the evaluation of CFD and correlations, an experimental data from Mokry *et al.*, 2010 & Mokry *et al.*, 2011 having 362 data points were selected. The selected data points cover a mass flux range of 300 -1600 kg/m² s, a heat flux range of 150-1000 kW/m², a pressure 240 bar and a diameter 10 mm. Out of 362 data points, 141 data points belongs to heat transfer enhancement and 221 data points belong to heat transfer deterioration. First, the experimental conditions are numerically simulated using CFD and 11 correlations identified from the literature are evaluated in the interest of determining the best correlation for the upward vertical flow at the supercritical pressure.

3.3 Comparison of CFD and correlations predictions with experimental data for heat transfer enhancement zone.

The selected 141 experimental data obtained from the literature for the heat transfer enhancement zone is shown in Table 1. It covers the range of the heat flux and mass flux ratio from 0.27 to 0.48.

Table 1 shows the heat flux and mass flux details for the heat transfer enhancement zone.

SL.No	Diameter (mm)	Heat flux (q) kW/m ²	Mass flux(G) kg/m ² s	Pressure(bar)	q/G ratio	Data points (nos)
01	10	141	504	241	0.279	29
02	10	190	498	241	0.38	33
03	10	590	1503	241	0.39	34
04	10	484	1002	241	0.48	45

The wall temperature predictions obtained by CFD and correlations were compared with the 141 experimental data points belonging to heat transfer enhancement zone as summarized in Table 2 (shown in Appendix). In the present work, 11 established correlations such as Dittus- Boelter, 1930; McAdams, 1942; Griem, 1996; Jackson and Hall, 1979; Shitsman 1968; Bishop *et al.*, 1964; Yamagata *et al.*, 1972; Mokry *et al.*, 2011; Zhu *et al.*, 2009; Watts & Chou, 1982 and Ornatsky *et al.*, 1971 were chosen for comparison. A visual basic code had been developed for predicting the wall temperature using correlations and for ranking the correlations and CFD predictions based on their prediction accuracies. Table 2 provides the wall temperature predicted by CFD and six correlations during heat transfer enhancement conditions. Table 3 provides the ranking information of CFD and empirical correlations on wall temperature prediction accuracies based on number of wall temperature points deviated with 141 experimental data points covering pseudocritical region where there is heat transfer enhancement (no heat transfer deterioration). Among the 11 correlations, Zhu *et al.* (2009), Jackson and Hall, (1974) and Mokry *et al.* (2011) shows the best agreement with 141 nos of data points, followed by Watts and Chou, (1982), Shitsman, (1968) and CFD correlations with 139, 138 and 137 number of data points at less than +/-3°C error level respectively. It is found that the CFD predictions have better agreement with 141 number of experimental data points with 100% of the predictions at less than +/-5°C error level. Fig. 10 provides the histogram of CFD and empirical correlations on wall temperature prediction accuracy based on percentage of error deviation in comparison with 141 experimental data points covering pseudo critical region where there is heat transfer enhancement (no heat transfer deterioration). Among the 11 correlations, CFD shows the best agreement with 141 number of experimental data points at less than +/-5 °C error level, along with Yamagata *et al.* (1972); Bishop *et al.* (1964); Watts and Chou (1982); Shitsman (1968); McAdams (1942) and Griem (1996) correlations with 100 % of predictions. Fig. 11 depicts the comparison of wall temperature predicted by CFD and Mokry *et al.*, (2011) correlation with experimental data for a typical heat transfer enhancement case. It is found that, wall temperature

predicted by both correlation and CFD are closely matches with experimental data. This is due to absence of non-linearity behavior of wall temperature.

Table 3 Typical comparison of wall temperatures predicted by CFD and selected correlations with 141 experimental data of Mokry *et al.* (2011) (for heat transfer enhancement zone) in percentage.

Sl.no	Correlations ranking	Comparison of wall temperature predictions by CFD and Various correlations with expt. (data points in nos)			
		<±7%	<±5%	<±3%	<±1%
1	Mokry	0	0	141	106
2	Jackson	0	0	141	106
3	McAdams	0	141	130	93
4	Watts & Chou	0	141	139	91
5	Griem	0	141	119	90
6	Dittus	0	141	132	83
7	Shitsman	0	141	138	82
8	Ornatsky	141	139	20	74
9	CFD	0	141	137	70
10	Zhu	0	0	141	69
11	Bishop	0	141	140	62
12	Yamagata	0	141	122	42

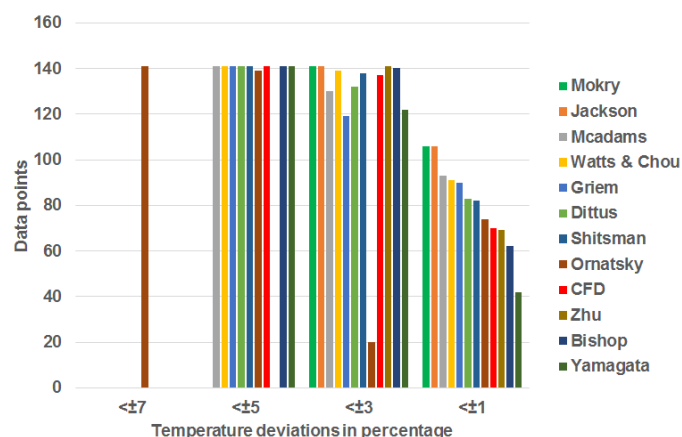


Fig. 10 Histogram for comparing the 141 experimental data with 11 correlations in the heat transfer enhancement zone.

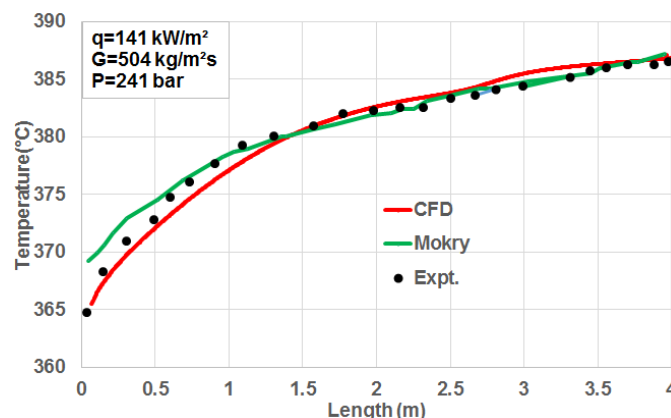


Fig. 11 Comparison of wall temperature predicted by CFD and by Mokry *et al.* (2011)'s Correlation for mass flux with that of experiment.

3.4 Comparison of CFD and correlations predictions with experimental data for heat transfer deterioration zone

The selected 221 experimental data points obtained from the literature for the heat transfer deteriorated zone is shown in Table 4. It covers the range of the heat flux and mass flux ratio from 0.58 to 0.83.

Table 4 shows the heat flux and mass flux details for the heat transfer deterioration zone.

Sl. No	Diameter (mm)	Heat flux (q) kW/m ²	Mass flux (G) kg/m ² s	Pressure (bar)	q/G ratio	Data points (nos)
01	10	289	499	241	0.58	43
02	10	334	499	241	0.67	63
03	10	686	994	241	0.69	30
04	10	166	206	241	0.805	39
05	10	826	1000	241	0.83	46

The wall temperature predictions obtained by CFD and 11 correlations were compared with the 221 experimental data points belonging to heat transfer deterioration zone as summarized in Table 5 (shown in Appendix). Table 6 provides the ranking information of CFD and empirical correlations on wall temperature prediction accuracies based on number of wall temperature points deviated with 221 experimental data points covering pseudocritical region where there is heat transfer deterioration. Table 6 provides the histogram ranking information of CFD and empirical correlations on wall temperature prediction accuracy based on percentage of error deviation in comparison with 221 experimental data points covering pseudocritical region where there is heat transfer deterioration. Among the 11 correlations, CFD shows the best agreement at less than +/-1°C error level followed by Zhu *et al.* (2009); Ornatsky *et al.* (1971); Jackson and Hall (1979) and Mokry *et al.* (2011) correlations. At less than +/-3°C level, Zhu *et al.* (2009) predicts 147 data points. At less than +/-5°C level, Zhu *et al.* (2009) predicts 192 number of data points accurately and followed by CFD and Watts and Chou (1982) with 171 & 165 data points respectively. At less than +/-7°C level, Zhu *et al.* (2009) predicts 205 number of data points accurately and followed by CFD, Watts and Chou (1982) with 190 & 188 data points respectively. At less than +/-10°C level, Zhu *et al.* (2009) predicts 211 number of data points accurately and followed by CFD, Watts and Chou (1982) with 208 data points. Among the 11 correlations, Zhu *et al.* (2009) shows the best agreement at less than +/-10°C, +/-7°C, +/-5°C and +/-3°C error level followed by CFD, Watts and Chou (1982) and Mokry *et al.* (2011) correlations.

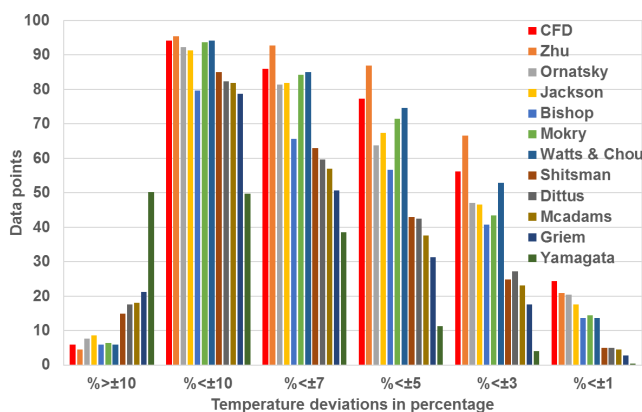


Fig. 12 Histogram for comparing the 221 experimental data with 11 correlations in the deteriorated heat transfer zone.

At less than +/-3°C level, Zhu *et al.* (2009) predicts 147 of data points accurately and followed by CFD and Watts & Chou with 124 & 117 data points respectively. It is also found that the CFD predictions have best agreement with experimental data at less than +/-1°C error level with 54 data points of the predictions and followed by Zhu *et al.* (2009) and Ornatsky *et al.* (1971) with 46 and 45 data points respectively. Fig. 12 provides the histogram of CFD and empirical correlations on wall temperature prediction accuracy based on percentage of error deviation in comparison with 221 experimental data points covering pseudocritical region where there is heat transfer deterioration. CFD shows best agreement with experimental data at less than +/-1 % and better agreement with experiment data at +/-10°C, +/-7 °C, +/-5 °C and +/-3°C. Fig. 13 depicts the comparison of wall temperature predicted by CFD and Zhu *et al.* (2009)'s correlation with that of experiment Mokry *et al.* (2011).

experimental data (Mokry *et al.*, 2011) for a typical heat transfer deterioration case. It is found that, unlike correlations prediction, the sudden rise in temperature is clearly predicted by CFD.

Table 6 Typical comparison of wall temperatures predicted by CFD and selected correlations with 221 experimental data (for heat transfer deterioration zone) in percentage.

Sl.no	Correlations ranking	Comparison of wall temperature predictions by CFD and various correlations with expt. (data points in nos)					
		>±10 %	<±10 %	<±7 %	<±5 %	<±3 %	<±1 %
1	CFD	13	208	190	171	124	54
2	Zhu	10	211	205	192	147	46
3	Ornatsky	17	204	180	141	104	45
4	Jackson	19	202	181	149	103	39
5	Mokry	14	207	186	158	96	32
6	Bishop	13	176	145	125	90	30
7	Watts & Chou	13	208	188	165	117	30
8	Shitsman	33	188	139	95	55	11
9	Dittus	39	182	132	94	60	11
10	Mcadams	40	181	126	83	51	10
11	Griem	47	174	112	69	39	6
12	Yamagata	111	110	85	25	9	1

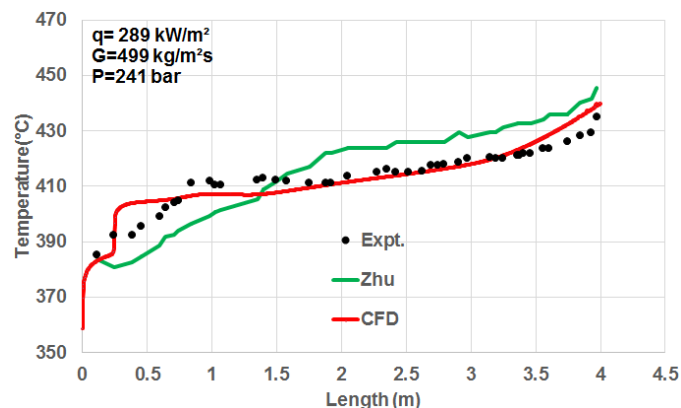


Fig. 13 Comparison of wall temperature predicted by CFD and by Zhu *et al.* (2009)'s correlation for mass flux with that of experiment Mokry *et al.* (2011).

4. CONCLUSIONS

The present work investigates the heat transfer in supercritical fluids by CFD and compares its prediction with various correlations available in literature. A two-dimensional axis-symmetric model has been considered. In order to evaluate the accuracy of the present model, the experimental data available in literature has been selected for validation. The computational domain is discretized with a non-uniform mesh of 120 nodes along the radial direction and 1200 uniform nodes along the axial direction after performing grid independency test. It is found that SST k- ω model captures heat transfer behavior at both enhancement and deterioration regions when compared with other turbulence models. A 362 experimental data have been taken from various literatures covering normal, heat transfer enhancement and heat transfer deterioration regimes for studying the capability of wall temperature prediction by CFD and various empirical correlations available in the literature. It is observed that under heat transfer enhancement zone the prediction accuracy by CFD based on wall temperature deviation and percentage error of wall temperature is the best along with Zhu *et al.* (2009), Mokry *et al.*, (2011) and Jackson and Hall (1974). At heat transfer deterioration zone, the prediction accuracy by CFD based on wall temperature

prediction (°C) is the best. None of the empirical correlations capable to predict the sharp gradient. Thus CFD can be used an alternate tool to predict the wall temperature and study the heat transfer characteristics (heat transfer deterioration and heat transfer enhancement) near pseudo critical region accurately.

NOMENCLATURE

b	Bulk fluid temperature (°C)
Bu	Buoyancy
C_p	Specific heat constant pressure (J/kg/k)
G	Mass flux(kg/m ² s)
G_r	Grashof number
h	Heat transfer coefficient (kW/m ²)
i, j	Direction of vectors
q	Heat flux (kW/m ²)
q_c	Limit heat flux (kW/m ²)
Nu	Nusselt number
Pr	Prandtl number
Re	Reynolds number
T_{pc}	Pseudocritical temperature (°C)
u	Velocity component (m/s)

Greek symbols

ρ	Density(kg/m ³)
k	Turbulent kinetic energy (m ² /s ²)
ω	Specific turbulence dissipation rate (1/s)
μ_t	Turbulent viscosity (kg/m/s)
ε	Rate of dissipation of k (m ² /s ³)
τ	Shear stress(kg/m/s ²)

Abbreviations

CFD	Computational Fluid Dynamics
HTE	Heat Transfer Enhancement
HTC	Heat Transfer Coefficient
HTD	Heat Transfer Deterioration
NHT	Normal Heat Transfer
SC	Supercritical
SST	Shear Stress Transport

REFERENCES

Bishop, A.A., Krambeck, F.J., and Sandberg, R.O., 1964, "High temperature supercritical water loop -PART III- Forced convection heat transfer to superheated steam at high pressure and high Prandtl numbers," *Westinghouse*, WCAP-2056.

Cheng, X., Schulenberg, T., Bittermann, D., and Rau, P., 2003, "Design analysis of core assembly for supercritical pressure conditions" *Nucl. Eng. Des.*, **223**, 279–294.
[https://doi.org/10.1016/S0029-5493\(03\)00059-1](https://doi.org/10.1016/S0029-5493(03)00059-1)

Dittus, F.W., and Boelter, L.M.K., 1930, "Heat transfer in automobile radiators of the tubular type," *University of California Publications in Engineering*, **2**, 443.
[https://doi.org/10.1016/0735-1933\(85\)90003](https://doi.org/10.1016/0735-1933(85)90003)

Griem, H., 1996, "A new procedure for the prediction of forced convection heat transfer at near- and supercritical pressure," *Heat and Mass Transfer (Warme und Stoffübertragung)*, Springer-Verlag Publishing House, **31** (5), 301–305.

Jackson J., and Hall W., 1979, "Forced convection heat transfer to fluids at supercritical pressure," *Turbulent Forced Convection in Channels Hemisphere Publishing Corp and Bundles*, New York, NY, USA, 563-611.

Jaromin.M., and Anglart, H., 2013, "A numerical study of heat transfer to supercritical water flowing upward in vertical tubes under normal and deteriorated conditions," *Nuclear Engineering and Design*, **264**, 61–70.
<https://doi.org/10.1016/j.nucengdes.2012.10.028>

McAdams, W.H., 1942, "Heat Transmission," 2nd edition, *McGraw-Hill*, New York, NY, USA, 459 pages.

Mokry, Pioro, Kirillov, and Gospodinov., 2010, "SC water heat transfer in a vertical bare tube," *Nuclear Engineering and Design*, **240**, 568–576.
<https://doi.org/10.1016/j.nucengdes.2009.09.003>

Mokry, S., Pioro, I., Farah, A., King, K., Gupta, S., Peiman., W and Kirillov, P., 2011, "Development of supercritical water heat transfer correlation for vertical bare tubes," *Nuclear Engg. Design*, **241**, 1126-1136.
<http://dx.doi.org/10.1016/j.nucengdes.2010.06.012>

Marcin Karol Rowinski, Jiyun Zhao, Timothy John White, Yeng Chai Soh., 2017, "Numerical investigation of supercritical water flow in a vertical pipe under axially non-uniform heat flux," *Progress in Nuclear Energy*, **97**, 11-25.
<https://doi.org/10.1016/j.pnucene.2016.12.009>

Ornatskij, A.P., Glushchenko, L.F., and Kalachev, S.I., 1971, "Heat transfer with rising and falling flows of water in tubes of small diameter at supercritical pressures," *Therm. Eng.*, **18**(5), 137–141.

Pioro, I. L., and Duffey, R.B., 2005, "Experimental heat transfer in supercritical water flowing inside channels (survey)," *Nucl. Eng. Des.*, **235**, 2407-2430.
<https://doi.org/10.1016/j.nucengdes.2005.05.034>

Shitsman, M.E., 1968, "Temperature conditions in tubes at supercritical pressures," *Thermal Engineering*, **15**(5), 72.

Tao Zhi, Cheng Zeyuan, Zhu Jianqin and Li Haiwang., 2016, "Effect of turbulence models on predicting convective heat transfer to hydrocarbon fuel at supercritical pressure," *Chinese Journal of Aeronautics*, **29**(5), 1247–1261.
<https://doi.org/10.1016/j.cja.2016.08.007>

Watts, M.J., and Chou, C.T., 1982, "Mixed convection heat transfer to supercritical pressure water," *Proceedings of the 7th International Heat Transfer Conference, Munchen, Germany*, **3**(6–10), 495–500.

Wen, Q.L., and Gu, H.Y., 2010, "Numerical simulation of heat transfer deterioration phenomenon in supercritical water through vertical tube," *Annals of Nuclear Energy*, **37**, 272–1280.
<https://doi.org/10.1016/j.anucene.2010.05.022>

Yamagata, K., Nishikawa, K., and Hasegawa, S., 1972, "Forced convective heat transfer to supercritical water flowing in tubes," *International Journal of Heat & Mass Transfer*, **15** (12), 2575–2593.
[https://doi.org/10.1016/0017-9310\(72\)90148-2](https://doi.org/10.1016/0017-9310(72)90148-2)

Zhu, X., Bi, Q., Yang, D., and Chen, T., 2009, "An investigation on heat transfer characteristics of different pressure steam-water in vertical upward tube," *Nuclear Engg. Design*, **239**, 381-388.
<https://doi.org/10.1016/j.nucengdes.2008.10.026>

Zhi Shang, and Shuo Chen., 2011, "Numerical investigation of diameter effect on heat transfer of supercritical water flows in horizontal round tubes," *Applied Thermal Engineering*, **31**, 573-581.
<https://doi.org/10.1016/j.applthermaleng.2010.10.020>

Appendix:

Table 2 Typical comparison of wall temperatures predicted by CFD and selected correlations with experimental data of Mokry *et al.*, (2011) (for heat transfer enhancement Zone).

Sl.No	Length (m)	Mass Flux(G) kg/m ² s	Heat Flux (q) kW/m ²	q/G	Bulk Fluid Temperature °C	Inner wall Temperature °C							
						Expt.	CFD	Mokry	Jackson	Zhu	Mcadams	Watts & chou	Dittus
1	0.05	504	141	0.28	350.9	365.6	364.8	369.2	367.1	368.2	366.7	368.3	367.6
2	0.11	504	141	0.28	351.8	367.9	366.5	369.9	367.9	368.9	367.5	368.9	368.4
3	0.15	504	141	0.28	352.7	369.2	367.5	370.6	368.7	369.6	368.4	369.6	369.2
4	0.21	504	141	0.28	354.0	370.1	368.5	371.6	369.8	370.6	369.6	370.6	370.5
5	0.30	504	141	0.28	355.8	371.4	369.9	372.9	371.3	372.0	371.2	372.0	372.1
6	0.52	504	141	0.28	358.0	375.4	372.3	374.5	373.2	373.6	373.2	373.5	374.1
7	0.68	504	141	0.28	360.7	376.3	374.2	376.2	375.3	375.4	375.6	375.3	376.5
8	0.02	498	190	0.38	351.7	365.8	367.5	375.6	373.2	374.2	373.1	373.6	374.3
9	0.07	498	190	0.38	352.5	370.8	371.3	376.1	373.9	374.7	373.8	374.1	375.0
10	0.23	498	190	0.38	355.8	376.6	375.1	377.9	376.4	376.5	376.8	376.1	378.0
11	0.27	498	190	0.38	355.8	376.6	375.9	377.9	376.3	376.5	376.8	376.1	377.9
12	0.30	498	190	0.38	356.6	377.4	376.3	378.3	376.9	376.9	377.5	376.6	378.7
13	2.45	498	190	0.38	384.5	394.5	391.5	403.3	399.8	402.9	395.5	404.3	396.1
14	2.63	498	190	0.38	383.6	395.3	391.6	400.5	397.2	400.3	393.1	401.6	393.6
15	2.94	498	190	0.38	385.2	396.9	391.8	405.4	401.8	404.8	397.4	406.3	398.0
16	1.56	1503	590	0.39	375.4	391.8	387.0	393.0	394.7	387.9	389.8	395.7	396.4
17	1.61	1503	590	0.39	376.2	391.8	387.0	393.5	395.0	388.8	389.4	396.2	396.1
18	1.79	1503	590	0.39	377.9	391.8	387.0	394.4	395.1	390.7	388.8	397.1	394.9
19	1.84	1503	590	0.39	377.9	391.8	387.0	394.4	395.1	390.7	388.8	397.1	394.9
20	2.06	1503	590	0.39	378.7	395.9	387.2	394.7	394.9	391.7	389.5	397.4	393.9
21	2.22	1503	590	0.39	379.5	396.7	387.6	395.0	394.5	392.7	389.9	397.6	392.6
22	1.22	1002	484	0.48	375.6	401.9	387.6	403.1	399.2	394.2	397.8	402.0	399.1
23	1.40	1002	484	0.48	377.6	401.0	388.4	403.5	399.2	396.5	396.4	402.8	397.5
24	1.43	1002	484	0.48	377.6	401.0	388.7	403.5	399.2	396.5	396.4	402.8	397.5
25	1.57	1002	484	0.48	378.6	402.0	390.4	403.5	398.7	397.7	395.1	402.9	396.0
26	1.75	1002	484	0.48	379.6	402.0	392.4	403.1	397.8	399.0	393.3	402.9	394.0
27	1.78	1002	484	0.48	381.6	402.0	392.7	404.5	397.7	403.6	391.0	404.9	391.6
28	1.94	1002	484	0.48	380.7	403.1	393.7	402.9	396.8	400.8	391.2	403.0	391.8
29	2.08	1002	484	0.48	381.7	404.1	394.5	404.7	397.9	403.9	391.2	405.2	391.7
30	2.20	1002	484	0.48	382.7	405.1	395.2	409.1	401.8	408.2	394.0	409.9	394.6

Table 5 Typical comparison of wall temperatures predicted by CFD and selected correlations with experimental data Mokry *et al.* (2010) & Mokry *et al.* (2011) (for heat transfer deterioration Zone).

Sl.No	Length (m)	Mass Flux (G) kg/m ² s	Heat Flux (q) kW/m ²	Bulk Fluid Temperature °C	Inner wall Temperature °C							
					Expt.	CFD	Zhu	Ornatsky	Jackson	Bishop	Mokry	Watts & chou
1	0.11	499	289	353.8	385.3	383.1	383.5	403.4	382.9	384.8	387.8	377.7
2	0.24	499	289	357.6	392.2	387.4	380.8	404.8	386.0	387.8	392.5	383.7
3	0.37	499	289	360.7	392.2	403.9	382.6	405.6	388.9	390.2	396.5	382.4
4	0.46	499	289	363.2	395.4	404.3	384.8	405.9	391.2	392.0	399.7	383.6
5	0.60	499	289	366.4	399.2	404.8	388.6	405.7	394.1	394.1	403.5	386.4
6	0.64	499	289	368.9	402.3	405.0	391.7	405.1	396.4	395.5	406.4	389.6
7	1.13	499	334	378.5	425.0	418.1	412.9	411.8	406.2	407.5	428.9	416.9
8	1.23	499	334	380.0	423.5	419.5	414.6	407.1	403.8	407.2	425.0	417.6
9	1.31	499	334	380.0	425.0	420.9	414.6	407.1	403.8	407.2	425.0	417.6
10	1.34	499	334	381.5	426.5	421.3	418.3	403.7	403.0	409.1	423.0	416.3
11	1.50	499	334	380.0	426.5	423.4	414.6	407.1	403.8	407.2	425.0	417.6
12	1.53	499	334	380.0	426.5	423.9	414.6	407.1	403.8	407.2	425.0	417.6
13	2.43	994	686	387.5	445.1	436.7	450.4	436.1	439.2	444.5	462.7	457.7
14	2.58	994	686	386.2	447.8	440.6	446.3	430.9	433.7	439.4	457.4	451.9
15	2.65	994	686	388.8	447.8	442.3	454.1	440.9	444.2	449.1	467.5	462.9
16	2.74	994	686	388.8	449.1	445.1	454.1	440.9	444.2	449.1	467.5	462.9
17	2.82	994	686	388.8	450.4	447.7	454.1	440.9	444.2	449.1	467.5	462.9
18	3.11	994	686	391.5	457.1	458.7	460.9	449.7	453.0	457.3	476.0	472.2
19	1.71	206	166	386.3	460.6	436.8	447.5	422.9	427.5	440.9	459.8	442.2
20	1.80	206	166	387.9	460.6	438.1	452.1	428.1	433.0	446.7	465.8	454.6
21	1.88	206	166	389.4	459.1	440.8	456.3	432.9	438.1	451.8	471.2	458.3
22	2.06	206	166	388.0	459.2	445.1	452.4	428.4	433.4	447.0	466.2	454.8
23	2.13	206	166	389.5	459.2	448.5	456.5	433.2	438.3	452.1	471.5	458.6
24	2.17	206	166	389.6	457.7	450.1	456.6	433.2	438.4	452.2	471.6	458.6
25	3.46	1000	826	408.8	514.7	547.2	517.7	516.9	516.9	523.4	552.4	545.3
26	3.66	1000	826	417.6	525.7	561.8	532.7	536.7	534.8	540.8	569.4	563.8
27	3.80	1000	826	426.5	539.0	572.2	546.5	554.5	550.6	556.4	584.7	580.3
28	3.85	1000	826	426.5	543.4	576.2	546.5	554.5	550.6	556.4	584.7	580.3
29	3.91	1000	826	430.9	550.0	580.2	553.1	562.7	558.0	563.7	591.9	587.9
30	3.94	1000	826	430.9	554.4	583.4	553.1	562.7	558.0	563.7	591.9	587.9